PHYSICAL REVIEW D

PARTICLES AND FIELDS

THIRD SERIES, VOLUME 34, NUMBER 5 1 SEPTEMBER 1986

Strange-particle production in neutrino-neon charged-current interactions

N. J. Baker,* P. L. Connolly,† S. A. Kahn, M. J. Murtagh, R. B. Palmer,
N. P. Samios, and M. Tanaka
Brookhaven National Laboratory, Upton, New York 11973

C. Baltay, M. Bregman,‡ L. Chen,§ M. Hibbs,‡ R. Hylton, J. Okamitsu,** and A. C. Schaffer††
Columbia University, New York, New York 10027

M. Kalelkar
Rutgers University, New Brunswick, New Jersey 08903
(Received 13 March 1986)

We report a study of strange-particle production from 61 800 charged-current ν_μNe interactions in the Fermilab 15-ft bubble chamber. The observed sample consists of 2279 K^0, 1843 Λ (including 94 Σ^0), 93 $\bar{\Lambda}$, and 4 Ξ^-. We give inclusive production rates for each of these, as well as the rates for specific single-, double-, and triple-vee channels. From these we derive the rates for associated production of $s\bar{s}$ quark pairs, and for single-s-quark production via charm decay. The dependence of K^0 and Λ production on E_ν, Q^2, W^2, x_B, and y_B are given. Normalized distributions of Feynman x, rapidity, fragmentation variable z, and transverse momentum squared are obtained for K^0 and Λ, and compared with those for charged pions. QCD predictions on the behavior of $\langle P_T{}^2 \rangle$ are tested.

I. INTRODUCTION

In this paper we present the results of an analysis of neutral-strange-particle production in ν_μ charged-current interactions in the Fermilab 15-ft bubble chamber. Our study is based on 61 800 charged-current events, containing 4215 observed vees that make constrained fits to the hypotheses $K_S \to \pi^+\pi^-$, $\Lambda \to p\pi^-$, or $\bar{\Lambda} \to \pi^+\bar{p}$. This sample represents about an order of magnitude greater statistics than any previously published similar work.

It is believed that strange-particle production in charged-current neutrino interactions is dominated by associated production. This is because the d quark is the only valence quark that can participate in the interaction, and the Cabibbo-favored process then produces a u quark as the current jet. Other processes, such as single-strange-particle production from the sea, and charm-particle production and decay, are expected to make small contributions to the strange-particle signal. A study of neutral-strange-particle production mechanisms provides insight into these ideas.

Strange particles are also important for studying charm states, since the Cabibbo-favored decay of the c quark produces an s quark. The noncharm background is vastly reduced in a sample of events with neutral strange particles, permitting a search for many hadronic decay modes of charmed mesons and baryons. We have previously published[1] results on the semileptonic decay of charm particles, and results[2,3] on the decays $D^0 \to K^0\pi^+\pi^-$ and $\Sigma_c^{++} \to \Lambda_c^+\pi^+$ based on partial statistics.

In Sec. II of this paper we discuss the selection of events and other experimental details. Rates for the production of K^0, Λ, and $\bar{\Lambda}$ are presented in Sec. III. We also give the first measurement of the rates for Σ^0 production, and for production of more than one neutral strange particle. In Sec. IV we use the single- and double-vee rates to determine how much of the strange-particle production is due to associated production, and how much to single-s-quark production via charm decay. Section V shows inclusive distributions using leptonic variables, as well as single-particle distributions using hadronic variables, in order to investigate strange-particle production mechanisms. In Sec. VI we report the rate for the hitherto unobserved Ξ^- production, and a description of the rare Ξ^- events.

II. EXPERIMENTAL PROCEDURE

The beam used in this experiment was the Fermilab double horn-focused wide-band ν_μ beam. The primary proton beam was extracted at an energy of 400 GeV in a fast spill ($\sim$20 μsec) with an average intensity of 10^{13} protons per pulse incident on the production target. Positively charged secondary particles from the production target were focused by the two horns and allowed to decay in a 400-m decay space. The beam neutrinos originated

 ©1986 The American Physical Society

from the decays of π^+ and K^+ mesons in this decay tube. The detector was separated from the end of the decay space by a 1-km earth shield, in order to absorb all particles except the beam neutrinos. The resulting neutrino spectrum peaked at 23 GeV, with about 10% of the events above 100 GeV.

The detector was the Fermilab 15-ft bubble chamber filled with a "heavy" neon-hydrogen mixture (61% atomic neon or 76% molar neon). The chamber is roughly spherical with a diameter of 3.7 m and a total target mass of 25 tons. Events were photographed using three cameras, and a total of 134 000 pictures in each of the three views was taken.

The chamber liquid had a radiation length of 40 cm, so that electrons were readily identifiable through bremsstrahlung and characteristic spiral. This provided a clear distinction between γ pair production and neutral-strange-particle decay (V^0).

The film was scanned for all events having at least one V^0. These events were measured and processed through our version of the geometrical reconstruction program TVGP. A fiducial volume cut was made to remove events within 70 cm of the back wall of the chamber, as well as events more than 125 cm above or below the midplane of the chamber. Approximately 25% of the events were eliminated by this cut. The fiducial volume had a mass of 17 tons.

The interaction length for hadrons in the neon mixture was about 125 cm, so that hadrons typically interacted in the liquid, while muons left the chamber without interaction. The charged-current sample was defined as those events having a negatively charged leaving track with a momentum greater than 2 GeV/c. If an event had more than one such track, the fastest negative leaving track was chosen as the muon. No use was made of the single-plane external muon identifier because of excessive background during our run. A final requirement on the charged-current sample was that the total visible energy be greater than 10 GeV. This visible energy included the energy of the charged tracks at the primary vertex as well as all visible associated neutrals (γ's, V^0's, and neutron stars).

The only significant background in the charged-current sample was provided by neutral-current, K_L, and neutron interactions in which a negative hadron happened to leave the chamber without interacting, thereby faking a μ^-. Since the π^- and π^+ cross sections are the same on an isoscalar target such as neon, the ratio of leaving to interacting *positive* tracks provides a measure of the punch-through probability. (Most of the positive tracks are hadrons.) Using this ratio and multiplying by the number of negative interacting tracks, we can calculate the number of negative leaving tracks that are due to hadronic punch-through. We actually applied this technique as a function of momentum, finding that the background was greater at low momentum. This was the reason for our cut of 2 GeV/c on the μ^- momentum. For the charged-current sample as a whole, the average punch-through background was about 9.1%.

All of the measured V^0's and γ's were processed through the kinematic-fitting program SQUAW. For each V^0 the following hypotheses were tried as constrained fits to the production vertex: $K_S \to \pi^+\pi^-$, $\Lambda \to p\pi^-$, $\bar{\Lambda} \to \pi^+\bar{p}$, and $\gamma p \to (p)e^+e^-$. (Each measured γ was fitted only to the last of these hypotheses.) Fits were required to have two or three degrees of freedom, and a χ^2 less than 5 times the number of constraints. A V^0 was considered to be a γ if (a) the constrained γ fit was successful, (b) neither track interacted in the liquid, and (c) the unconstrained effective mass of the e^+e^- pair was less than 30 MeV. Only about 1% of the V^0 were taken to be γ's since, as noted earlier, the small radiation length of the chamber liquid permitted very reliable identification of electrons.

About 30% of the V^0's had an acceptable constrained fit for more than one hypothesis. To resolve these ambiguities, we examined the distributions of the cosine of the angle between the V^0 line of flight and the negative decay product in the rest frame of the V^0. This decay cosine must be isotropic for the spinless K_S, and also isotropic for the Λ and $\bar{\Lambda}$ if they have no longitudinal polarization. Fit ambiguities were resolved using an algorithm designed to make the decay cosine distributions as flat as possible: (a) for K_S/Λ ambiguities, the V^0 was selected to be a Λ if the probability for the Λ fit exceeded 0.5 times the probability for the K_S fit; (b) for $K_S/\bar{\Lambda}$ ambiguities, the V^0 was selected to be a K_S if the K_S probability exceeded 0.3 times the $\bar{\Lambda}$ probability; (c) for $\Lambda/\bar{\Lambda}$ ambiguities, the V^0 was selected to be a Λ if the Λ probability exceeded 0.5 times the $\bar{\Lambda}$ probability.

Figure 1 shows the decay cosine distributions after this algorithm is applied. The distributions are flat for the most part, but there is some departure from isotropy (especially for the Λ) in the first few bins. No selection algorithm can eliminate the anisotropy in both plots, suggesting that there is a systematic loss of events. We will return to this point in our discussion of corrections to the V^0 rate.

One further cut was made on the V^0 sample. The scanning efficiency for a V^0 is poor if the vee is very close to the vertex, since the decay prongs of the vee can be confused with charged tracks emanating from the primary vertex. We therefore required that all vees have a minimum length of 1 cm from the vertex. We also re-

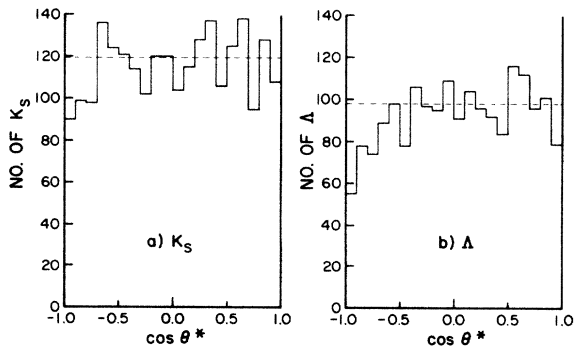

FIG. 1. Distribution of the cosine of the angle between the V^0 line of flight and the negative decay product in the V^0 rest frame, for (a) K_S and (b) Λ. The dashed line was used to estimate the loss in the depleted bins.

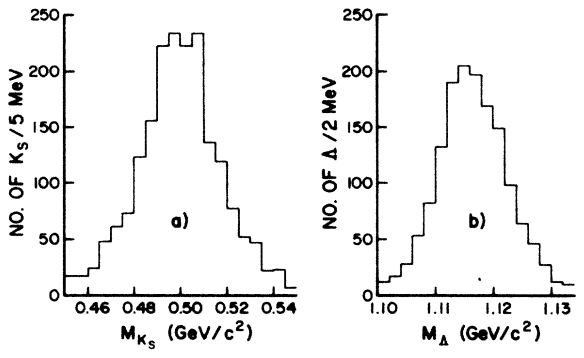

FIG. 2. Unconstrained-effective-mass distributions for (a) K_S and (b) Λ. These plots give a measure of the experimental mass resolution.

moved all vees that were less than 10 cm from the chamber wall.

After applying all these selection criteria, we obtained a final sample of 2279 K_S, 1843 Λ, and 93 $\bar{\Lambda}$ associated with charged-current events. Figure 2 shows the unconstrained-effective-mass distributions for the vees selected as K_S and Λ. The resolutions for the K_S and Λ masses (i.e., the σ of the distributions) are 14 and 6 MeV, respectively.

For the rest of this paper the sample of events obtained as described above will be referred to as the strange charged-current (SCC) sample. As discussed later, it is instructive to compare the properties of this sample with charged-current events as a whole. For this reason we also measured some charged-current events selected randomly, without regard to the presence or absence of strangeness. This control sample will be referred to as the random charged-current (RCC) sample. It was processed in a manner identical to that for the SCC sample, and subjected to the same selection criteria. After all cuts, the RCC sample consisted of about 2500 events.

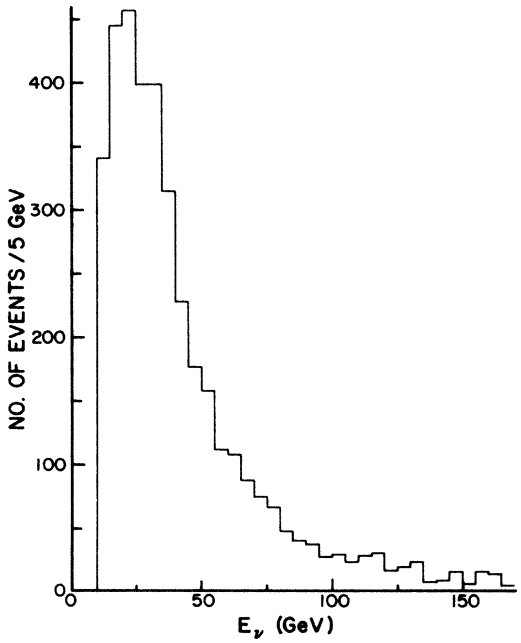

FIG. 3. Neutrino energy distribution for the strange charged-current sample. The measured (visible) energy was corrected for undetected neutrals using a method based on transverse-momentum balance.

The measurement of events in both samples included all the charged tracks at the primary vertex, and all the visible associated neutrals (γ's, vees, and neutron interactions). We estimate that approximately 80% of the hadronic energy is visible. To correct for the missing energy we employed the method proposed by Grant,[4] modified for use with heavy liquid. The average hadron-energy correction was $(23\pm3)\%$, corresponding to an average $(10\pm1)\%$ correction to the visible energy. Figure 3 shows the corrected neutrino event energy distribution for the SCC sample, with an average neutrino energy of 46 GeV. The corresponding distribution for the RCC sample is very similar, and has the same mean.

III. PRODUCTION RATES

To calculate V^0 production rates, it was necessary to correct the observed number of vees for various efficiencies and backgrounds. The corrected numbers were given by

$$N_{\text{corr}}=N_{\text{obs}}\frac{C_1C_2C_3C_4C_5C_6C_{10}}{C_7C_8C_9}\ .$$

The ten correction factors are summarized in Table I, and here we discuss the more important ones.

The geometric detection efficiency, which was momentum dependent, was calculated using the minimum and maximum length cuts discussed in the preceding section, along with the known lifetimes.[5] Another inefficiency was that due to vees undergoing interaction before decay. For each observed vee traveling a distance l before decaying, the probability that it did not interact is e^{-l/l_0}, where l_0 is the interaction length. We used $l_0=125$ cm for K_S, and $l_0=100$ cm for Λ and $\bar{\Lambda}$. Each vee was then weighted for geometric efficiency and noninteraction efficiency. A check of our procedure is provided by examining the weighted proper decay length distributions, which are shown in Fig. 4. Also shown are exponential fits to the distributions, which were made using all the data points except the first bin. For the K_S, the fit from $c\tau=1.0$ to 9.0 cm yielded a χ^2 of 3.6 for 6 degrees of freedom, and a mean proper decay length of $c\tau=2.70\pm0.12$ cm. For the Λ, the fit was from $c\tau=2.0$ to 22.0 cm, and yielded a χ^2 of 5.8 for 8 degrees of freedom, with a mean proper decay length of 8.7 ± 0.5 cm. Both fits are excellent, and the proper decay lengths are consistent with the known values.[5] The fits were extrapolated to $c\tau=0$, as shown in Fig. 4, and the low-lifetime loss was calculated by subtracting the first bin from the extrapolation.

The entire vee sample was double scanned, and a random scan efficiency of $(95\pm2)\%$ for the vees was obtained. However, there was also a systematic loss of vees. As discussed in the preceding section, the decay cosine distributions (see Fig. 1) revealed a depletion of events, especially for the Λ. The depletion is primarily due to

TABLE I. Correction factors to observed V^0 production.

Correction factor	K^0	Λ
Geometric detection efficiency (C_1)	1.147±0.004	1.117±0.003
Interaction before decay (C_2)	1.17 ±0.02	1.16 ±0.03
Low-lifetime loss (C_3)	1.15 ±0.02	1.11 ±0.02
Slow decay prong (C_4)	1.03 ±0.01	1.06 ±0.01
Punch-through background (C_5)	0.909±0.010	0.909±0.010
Fake fits (C_6)	0.95 ±0.02	0.95 ±0.02
Random scan efficiency (C_7)	0.95 ±0.02	0.95 ±0.02
Reconstruction efficiency (C_8)	0.96 ±0.02	0.96 ±0.02
Branching ratio (C_9)	0.343±0.001	0.642±0.005
Ambiguity resolution (C_{10})	1.04 ±0.02	0.97 ±0.02
Average total weight	4.56 ±0.23	2.18 ±0.12

vees with a slow π^- (below ~ 100 MeV/c). A vee with a very short negative prong can look like an isolated proton track, with a reduced efficiency for being recognized as a vee. Even if the vee is found, a slow π^- has a length of only a few cm, and therefore has an enhanced probability of measurement failure. These problems are much less severe when there is a slow positive track. Then one sees an isolated *negative* track, which cannot be dismissed as a floating proton. Furthermore, when the slow positive track is a proton, there is virtually no reconstruction problem, since such protons almost invariably stop in the chamber, and their momentum is obtained very accurately from range.

We assume that the decay cosine distributions must be isotropic in reality. By extrapolating the observed distributions, we calculated the loss in the depleted bins to be (3±1)% for the K_S, and (6±1)% for the Λ.

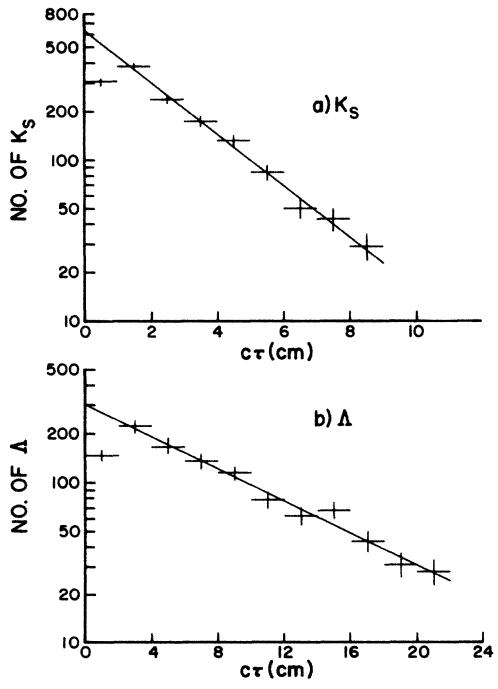

FIG. 4. Proper lifetime distributions for (a) K_S and (b) Λ. The events were weighted for momentum-dependent geometric efficiency, as well as for probability of interaction before decay. The line is a linear fit using all points but the first bin.

The ambiguity resolution procedure described in the preceding section was designed to render the decay cosine distributions as flat as possible. For K_S-Λ ambiguities, the algorithm generally favored the Λ over the K_S. It is likely, therefore, that the Λ sample includes some K_S contamination. To estimate this contamination, we make use of the $\bar{\Lambda}$ sample, since the K_S contamination should be the same in both samples by symmetry. We generated a separate, special selection algorithm in which the $\bar{\Lambda}$ was treated identically to the Λ for ambiguity resolution. The decay cosine distributions for the $\bar{\Lambda}$ then displayed an excess of 66±10 events in the kinematic region corresponding to K_S contamination. We assumed the same contamination in the Λ sample to calculate the ambiguity resolution correction factors shown in Table I.

For the selection algorithm that we actually used for our data sample, the $\bar{\Lambda}$ was disfavored in ambiguity resolution, so that there was little contamination of the $\bar{\Lambda}$ sample. In fact, the greater problem was that of loss of $\bar{\Lambda}$. To estimate the true number of $\bar{\Lambda}$, we noted that our final Λ sample was 1.98 times the number of unique Λ fits. By symmetry, the ratio should be similar for $\bar{\Lambda}$, provided the Λ and $\bar{\Lambda}$ momentum spectra are similar, which is actually the case. We had 64 unique $\bar{\Lambda}$, so this argument suggests a true final sample of 127. Since our actual sample is 93 $\bar{\Lambda}$, we estimate an overall correction factor of 1.37±0.17.

The vees were also corrected for undetected decay modes using the known branching ratios.[5] In Table I the branching ratio for K^0 includes the factor of 2 for K_L, so that our rates are for all $K^0+\bar{K}^0$. The final average weights were 4.56±0.23 for K^0, 2.18±0.12 for Λ, and 3.08±0.41 for $\bar{\Lambda}$.

Inclusive V^0 production rates as a fraction of all charged-current events are shown in Table II. They are based on a total charged-current sample of 61 800±2800 events with $E_\nu > 10$ GeV and $P_\mu > 2$ GeV/c. The Λ rate includes those Λ's coming from Σ^0 decay. From the table we derive a ratio of the Λ to K^0 rate of 0.39±0.04.

In Table III we give the observed number of events and corrected rates for 11 specific single-, double-, and triple-V^0 channels. It should be noted that the rates cannot be

TABLE II. Total inclusive strange-particle production rates. The Λ rate includes Λ's coming from Σ^0 decay. The K^0 rate includes $K^0+\bar{K}^0$.

Particle	Observed	Corrected	Rate per charged-current event
K^0	2279	10392	0.168 ± 0.012
Λ	1843	4018	0.065 ± 0.005
$\bar{\Lambda}$	93	286	0.0046 ± 0.0008
Σ^0	94	713	0.011 ± 0.003
Ξ^-	4	36	$(5.8 \pm 3.6) \times 10^{-4}$

obtained merely by multiplying the number of observed events by appropriate average weights. Rather, it is necessary to solve 11 simultaneous equations; for example, the number of observed single-K^0 events is written as a sum over the true rates for each of the 11 channels times appropriate efficiencies for that channel being observed as single K^0.

Strange-particle production has been studied previously both in neutrino[6–13] and antineutrino[11–15] experiments. In Table IV we compare our results with some of these earlier measurements. It may be noted that we have significantly more events than any of the others. Although our rate for K^0 production is somewhat lower than most others, it should be pointed out that the experiments are not exactly comparable. In our experiment there are about twice as many interactions on neutrons than protons, because there are two valence d quarks in the former and only one in the latter. A deuterium experiment[13] has observed a significant difference in V^0 production on neutrons and protons (see Table IV). Moreover, as discussed in the next section, the K^0 rate increases with energy, explaining the high value seen by Ref. 12. Our results are in close agreement with an antineutrino experiment[15] which also used the 15-ft neon bubble chamber.

Double-V^0 production (see Table III) occurs at about a 2% rate both for K^0K^0 and $K^0\Lambda$. Other experiments are consistent with our rate, but their statistics are too low to warrant a detailed comparison. Triple-V^0 production is about a factor of 3 lower in rate than double-V^0 production.

In order to measure the Σ^0 production rate, we show in Fig. 5 the $\Lambda\gamma$ effective-mass distribution. There is a very clear signal at the Σ^0 mass. We have performed a fit to the distribution, using a Gaussian shape for the Σ^0, and a third-order polynomial background. The fit, which had a χ^2 of 23.5 for 24 degrees of freedom, is shown as the solid curve in Fig. 5, while the dashed curve indicates the fitted background. The Gaussian fit yielded a mass of $M = 1195 \pm 2$ MeV and $\sigma = 8 \pm 2$ MeV. The mass is consistent with that of the Σ^0, and the value of σ coincides with our mass resolution in the $\Lambda\gamma$ system at the Σ^0 mass. The fit yielded a total of 94 ± 25 Σ^0's where the error includes contributions from the statistical error, the errors in M and σ, and the uncertainty in the determination of the background.

To obtain the Σ^0 rate, it is necessary to weight the Σ^0 not only for the Λ detection efficiency, but for the γ as well. There are several sources of γ losses[16] (average weights given in parentheses): (a) geometric detection weight (1.33); (b) low-energy $e^{\pm}$ prongs (1.16); (c) short projected $e^{\pm}$ tracks on film (1.37); (d) poor $e^{\pm}$ track visibility (1.03); and (e) random γ scan efficiency (1.69). Some of these losses are correlated; the overall average weight for γ's was 3.18 ± 0.31. We then obtain a total inclusive Σ^0 production rate of $(1.1 \pm 0.3)\%$ as a fraction of all charged-current events. We also obtain the fraction of Λ coming from Σ^0 decay:

$$\frac{R(\nu_\mu + \mathrm{Ne} \to \mu^- + \Sigma^0 + \cdots)}{R(\nu_\mu + \mathrm{Ne} \to \mu^- + \Lambda + \cdots)} = (16 \pm 5)\% \ .$$

To our knowledge, this is the first measurement of the Σ^0

TABLE III. Single-, double-, and triple-V^0 production rates. Note that X does not contain a visible V^0. K^0 includes $K^0+\bar{K}^0$.

Reaction	Observed events	Rate per charged-current event
$\nu_\mu\mathrm{Ne} \to \mu^- K^0 X$ (single K^0 only)	1834	$(8.0 \pm 0.8) \times 10^{-2}$
$\mu^- \Lambda X$ (single Λ only)	1569	$(3.2 \pm 0.3) \times 10^{-2}$
$\mu^- \bar{\Lambda} X$ (single $\bar{\Lambda}$ only)	79	$(2.4 \pm 0.6) \times 10^{-3}$
$\mu^- K^0 K^0 X$	100	$(1.6 \pm 0.8) \times 10^{-2}$
$\mu^- K^0 \Lambda X$	205	$(2.3 \pm 0.4) \times 10^{-2}$
$\mu^- K^0 \bar{\Lambda} X$	6	$(1.4 \pm 0.5) \times 10^{-3}$
$\mu^- \Lambda\Lambda X$	20	$(1.6 \pm 6.9) \times 10^{-4}$
$\mu^- \Lambda\bar{\Lambda} X$	8	$(9 \pm 3) \times 10^{-4}$
$\mu^- K^0 K^0 K^0 X$	4	$(6 \pm 3) \times 10^{-3}$
$\mu^- K^0 K^0 \Lambda X$	8	$(6 \pm 2) \times 10^{-3}$
$\mu^- K^0 \Lambda\Lambda X$	5	$(1.8 \pm 0.8) \times 10^{-3}$

TABLE IV. Comparison of results on K^0 and Λ production by ν and $\bar{\nu}$. The rates (R_K and R_Λ) are inclusive rates as a fraction of all charged-current events. The numbers of V^0 (N_K and N_Λ) are the raw, observed numbers.

Reference	Reaction	$\langle E_\nu \rangle$ (GeV)	N_K	R_K	N_Λ	R_Λ	R_Λ/R_K
This expt.	νNe	46	2279	0.168±0.012	1843	0.065±0.005	0.39±0.04
12	νNe	103	203	0.230±0.017	98	0.057±0.007	0.25±0.03
13	νn	62	234	0.208±0.016	157	0.071±0.007	0.34±0.05
13	νp	62	154	0.177±0.016	77	0.043±0.006	0.24±0.04
11	νp	~45	23	0.15 ±0.04	4		
10	νp	43	359	0.175±0.009	180	0.045±0.004	0.26±0.03
8	νp	~45	89		58		
7	νp	~45	19		20		
9	νd	~3	13	0.024±0.009	26	0.028±0.010	1.17±0.61
6	ν-Freon	~3	14		40		
12	$\bar{\nu}$Ne	81	64	0.219±0.028	37	0.065±0.012	0.30±0.05
13	$\bar{\nu} n$	45	95	0.219±0.025	68	0.082±0.012	0.37±0.07
13	$\bar{\nu} p$	45	193	0.222±0.018	113	0.070±0.008	0.32±0.05
15	$\bar{\nu}$Ne	~45	350	0.164±0.009	257	0.063±0.004	0.38±0.03
11	$\bar{\nu} p$	~45	88	0.151±0.032	46	0.045±0.009	0.30±0.09

production rate in neutrino interactions. From a νp experiment, Berge *et al.* reported[8] that six $\Lambda\gamma$ mass combinations in the Σ^0 region accounted for between 50 and 100% of the Λ production.

We have also measured Ξ^- production, which we discuss separately in Sec. VI, because of the special procedures that were needed.

IV. RATES FOR ASSOCIATED PRODUCTION AND SINGLE-*S*-QUARK PRODUCTION

In this section we investigate the origin of strange-particle production in charged-current neutrino interactions. We remarked in the Introduction that the d quark is the only valence quark in the nucleon that can participate in such interactions, and the Cabibbo-favored process then produces a u quark. Therefore the primary mechanism for strange-particle production is expected to be associated production of an $s\bar{s}$ quark pair. There is, however, a source of single-s-quark production, and that is via charm. The interaction of the d quark can produce a c quark, and the Cabibbo-favored decay of the c quark yields an s quark. There is no simple source for single-$\bar{s}$ production; one possibility is an interaction off a $\bar{u}$ quark in the sea, followed by disfavored production of $\bar{s}$.

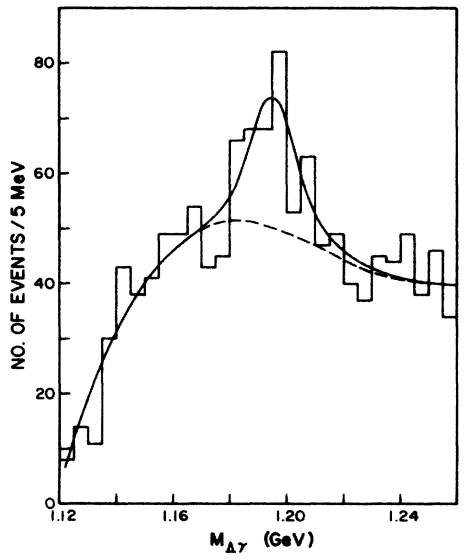

FIG. 5. Effective-mass distribution of $\Lambda\gamma$ system, using fitted Λ and γ. The solid line is a fit using a Gaussian shape for the Σ^0, and a polynomial background. The dashed line shows the background level.

Our aim is to use our measured rates for single- and double-vee production to derive (a) R_{AP}, the rate for associated production of s and $\bar{s}$ in charged-current neutrino interactions, and (b) R_S, the rate for single-s production (via charm). We define the following probabilities. (a) P_{SM} is the probability that an s quark appears as a meson. Then $(1-P_{SM})$ is the probability that an s quark appears as a baryon. (b) P_{ASM} is the probability that an $\bar{s}$ quark appears as a meson, so that $(1-P_{ASM})$ is the probability that it appears as an antibaryon. (c) P_{MV} is the probability that a strange meson will appear electrically neutral, i.e., K^0, not $K^\pm$. (d) P_{BV} is the probability that a strange baryon will appear electrically neutral, i.e., Λ, not $\Sigma^\pm$.

We assume that $P_{MV}=0.5$, because we have an isoscalar target, with equal numbers of u, d, $\bar{u}$, $\bar{d}$ quarks. Therefore an s or $\bar{s}$ quark has an equal chance of appearing as a charged or neutral K meson. We will also later examine the consequences of relaxing this assumption.

From these probabilities we can easily write expressions for the chance that an s or $\bar{s}$ quark will appear as a particular kind of vee. (a) The chance that an s quark will appear as a K^0 is $P_{SM}P_{MV}$. (b) The chance that an s quark will appear as a Λ is $(1-P_{SM})P_{BV}$. (c) The chance that an $\bar{s}$ quark will appear as a K^0 is $P_{ASM}P_{MV}$. (d) The chance that an $\bar{s}$ quark will appear as a $\bar{\Lambda}$ is $(1-P_{ASM})P_{BV}$.

By appropriately combining these probabilities with the rates R_{AP} and R_S, we can write expressions for the rates for single- and double-vee production. We have done so for the seven channels: single K^0, single Λ, single $\bar{\Lambda}$, K^0K^0, $K^0\Lambda$, $K^0\bar{\Lambda}$, and $\Lambda\bar{\Lambda}$. For these seven channels we have measured the rates with errors (see Table III) and so we can perform a fit to obtain our five unknowns. The best fit had a χ^2 of 1.39 for 2 degrees of freedom, and yielded the following results:

$$R_{AP}=0.195\pm0.014\ ,$$

$$R_S=0.050\pm0.015\ ,$$

$$P_{SM}=0.445\pm0.040\ ,$$

$$P_{ASM}=0.945\pm0.010\ ,$$

$$P_{BV}=0.414\pm0.029\ .$$

These results confirm that the dominant mechanism is associated production, which occurs at a 20% rate. Charm-particle production occurs at about a 5% rate, and since the μ^-e^+ rate[1] is 0.5%, our results imply that the average branching ratio of charm particles we produce into e^+ is of order 10%. This is a reasonable result, since the branching ratios into e^+ are known[5] to be 5% for the D^0, 19% for the D^+, and 4.5% for the Λ_c. It is also reasonable that we find P_{ASM} is close to 1. An $\bar{s}$ quark is much more likely to appear as a meson than as an antibaryon. To appear as an antibaryon it would have to pick up two antiquarks from the sea, whereas to appear as a meson it need only pick up one ordinary quark (u or d).

Next, we examine whether our assumption was reasonable that $P_{MV}=0.5$. We fix the rates and probabilities at the values obtained above, and permit only P_{MV} to vary. The best fit yields $P_{MV}=0.50\pm0.04$, and the same result is obtained if all the variables are set free.

Finally, we can use these results to predict the rate for the "anomalous" $\Lambda\Lambda$ channel. This channel is anomalous because it requires that either (a) double associated production occurs, or (b) associated production and charm production both take place. Our fitted results predict a rate for the latter possibility of about 2.4×10^{-4}, while our measured rate from Table III is $(1.6\pm6.9)\times10^{-4}$.

V. DIFFERENTIAL DISTRIBUTIONS

To investigate strange-particle production mechanisms we consider next the differential distributions for K^0 and Λ production. Variables that describe the production process can be divided into two classes: (a) those that characterize the event as a whole and (b) those that are specific to a particular produced particle.

In the first category we examine the following variables. (i) E_ν is the corrected neutrino energy. (ii) $Q^2=2E_\nu(E_\mu-P_{L\mu})-m_\mu{}^2$, the invariant square of the four-momentum transfer from the neutrino to the muon. In this expression the muon energy E_μ and longitudinal momentum $P_{L\mu}$ are in the laboratory frame. (iii) $W^2=2m_p(E_\nu-E_\mu)+m_p{}^2-Q^2$, the invariant square of the hadronic system's effective mass. (iv) $x_B=Q^2/2m_p(E_\nu-E_\mu)$, the Bjorken scaling variable. (v) $y_B=(E_\nu-E_\mu)/E_\nu$, the fractional energy transfer to the hadrons.

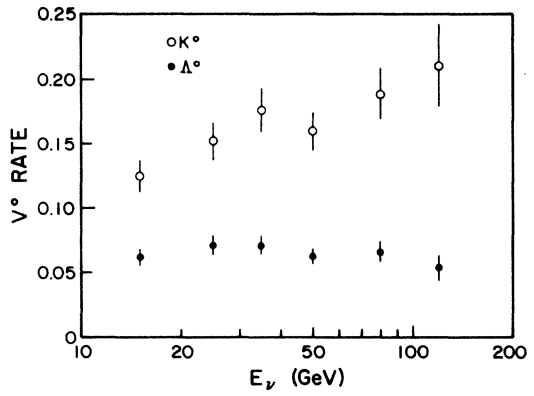

FIG. 6. Inclusive V^0 production rates as a function of incident neutrino energy. The open circles are for K^0, and the solid circles are for Λ.

In Figs. 6–9 we show the K^0 and Λ production rates as functions of these variables. To produce these figures we obtained distributions of each variable for the SCC and RCC samples separately, and then divided them after appropriate normalization. However, since there is a threshold for strangeness production, we made a cut requiring $W>2$ GeV on both the SCC and RCC samples before doing the comparison.

The figures reveal striking differences between the K^0 and Λ. The production rate of Λ is essentially independent of E_ν, Q^2, W^2, and y_B, while the K^0 rate increases sharply with all of these variables. A simple interpretation is that the Λ is produced in the target fragmentation region, and is generally independent of the energy of the W^+ coming from the leptonic vertex. By contrast, the K^0 is in the current jet where the s (or $\bar{s}$) quark is picked up from the sea, and this process is increasingly favored as the W^+ energy rises. In this context we observe from Fig. 9(a) that both the K^0 and Λ rates are independent of x_B. Recall that x_B is the fraction of the nucleon momen-

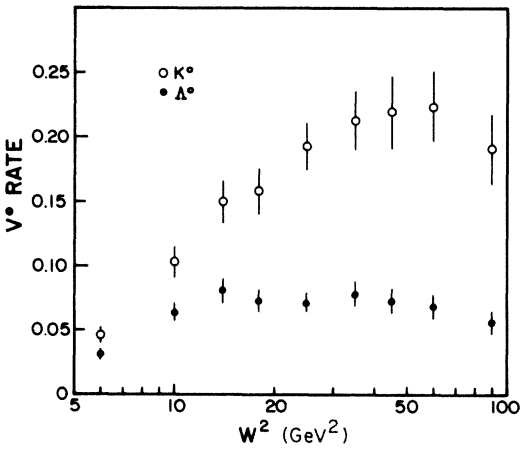

FIG. 7. Inclusive V^0 production rates as a function of W^2, the invariant square of the hadronic effective mass. The open circles are for K^0, and the solid circles are for Λ.

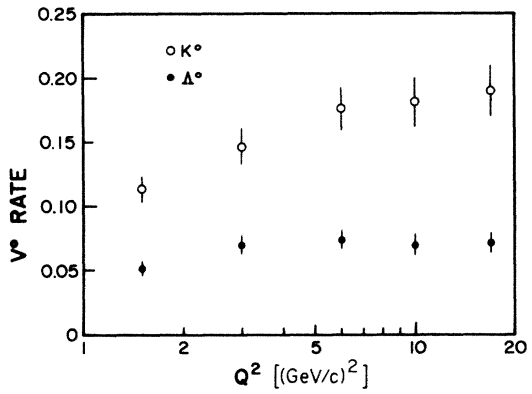

FIG. 8. Inclusive V^0 production rates as a function of Q^2, the invariant square of the four-momentum transfer from the neutrino to the muon. The open circles are for K^0, and the solid circles are for Λ.

tum carried by the struck quark. Hence the production of K^0 is determined primarily not by the struck quark, but rather by the momentum of the W^+.

Additional information is obtained when we consider the second category of variables—those describing a particular particle.

(i) $x_F=2P_L^*/W$, the Feynman-x variable. Here, P_L^* is the longitudinal momentum of the particle in the hadronic center of mass, and W is the total hadronic effective mass as defined previously. The longitudinal direction is the line of flight of the W^+.

(ii) $y^*=\frac{1}{2}\ln[(E^*+P_L^*)/(E^*-P_L^*)]$, the particle's center-of-mass rapidity. Here, E^* is the particle's total energy in the hadronic center of mass.

(iii) z, the fraction of the total corrected hadronic laboratory energy carried by the particle.

(iv) P_T^2, the square of the momentum transverse to the W^+ direction.

Distributions in these four variables have been obtained for K^0 and Λ from the SCC sample, and for π^+ and π^- from the RCC sample. The distributions are normalized to the total number of charged-current events N_{CC} in each sample, so that the abscissa at any point represents the average multiplicity of the particular particle per unit interval of the variable.

Figure 10 shows the distributions in x_F. The Λ is very obviously in the backward direction characteristic of a target fragmentation process. The K^0 peaks in the central region, but there is an asymmetry in the forward direction as would be expected if the K^0 is produced in the current jet. We can see this more clearly in the asymmetry parameter

$$A=(N_F-N_B)/(N_F+N_B)\ ,$$

where N_F and N_B are the numbers of particles going forward and backward, respectively. We calculate $A=0.16\pm0.02$ for the K^0, and $A=-0.71\pm0.02$ for the Λ. These values are consistent with a recent neon experiment,[12] but significantly less than those reported from a hydrogen[10] and a deuterium[13] experiment. The pions in the RCC sample are produced mostly in a very narrow region around $x_F=0$. Their asymmetry parameters are $A=+0.004\pm0.012$ for π^+, and $A=-0.082\pm0.017$ for π^-.

A sensitive way to compare the production properties of the K^0 and $\pi^\pm$ is to examine the ratios of the normalized x_F distributions. Such a plot is shown in Fig. 11. The K^0/π^+ ratio unambiguously indicates enhanced production of K^0 in the forward region relative to π^+. The π^-/π^+ ratio reveals that π^- are more tightly bunched around $x_F=0$. It was mentioned in the Introduction that the W^+ interactions with a d quark in the nucleon produce a u quark. Since the π^+ includes a u quark while the π^- does not, it is not surprising that there is relatively more π^+ production in the current region. In the extreme backward direction, the apparent excess of π^+ over π^- may be due to proton contamination in the π^+ sample, since protons are identified only if they stop in the bubble chamber.

Normalized rapidity distributions are displayed in Fig. 12, and their ratios in Fig. 13. As with Feynman x, the rapidities show the pronounced backward production of Λ and slightly forward production of K^0. Rapidity, however, differs from x_F in that it depends both on longitudinal and transverse momentum, while x_F is essentially independent of P_T. At a given P_L^*, higher values of P_T are toward $|y^*|\sim0$. The K^0/π^+ ratio is enhanced near $|y^*|\sim0$, and the K^0 does have greater transverse momentum than the π^+ on the average. The π^-/π^+ ratio shows a rather monotonic decrease with rapidity; the

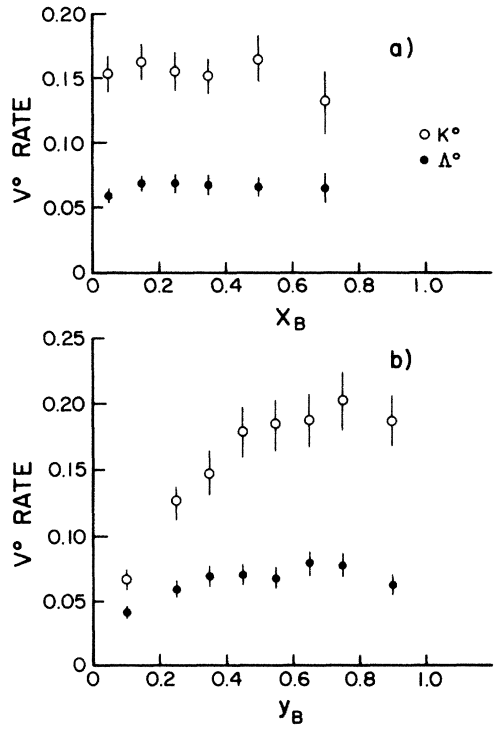

FIG. 9. Inclusive V^0 production rates as a function of the Bjorken scaling variables: (a) x_B, the fraction of the nucleon momentum carried by the struck quark, and (b) y_B, the fractional energy transfer to the hadron system. The open circles are for K^0, and the solid circles are for Λ.

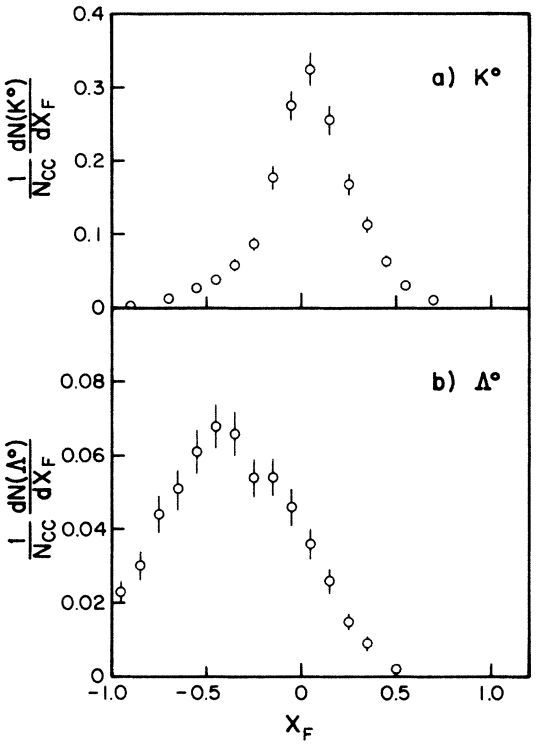

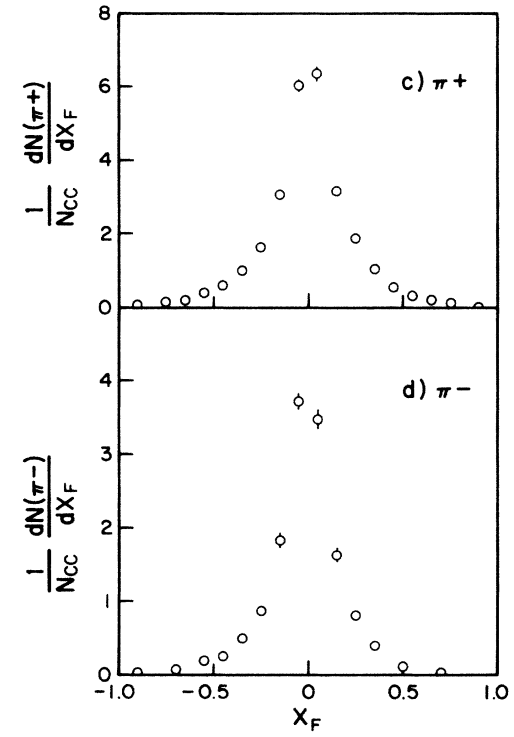

FIG. 10. Feynman-x distributions for (a) K^0, (b) Λ, (c) π^+, and (d) π^-, normalized to the total number of charged-current events. The pion distributions are from the random charged-current sample.

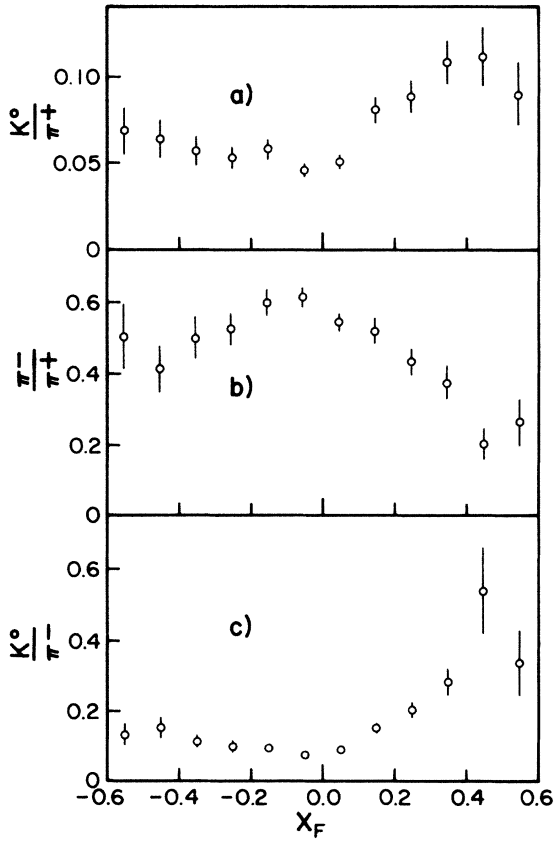

FIG. 11. Ratios of normalized Feynman-x distributions for (a) K^0/π^+, (b) π^-/π^+, and (c) K^0/π^-.

π^- have somewhat softer P_T and are more concentrated near $P_L^*=0$. Table V summarizes average values of P_T and other variables for K^0, Λ, π^+, and π^-.

Figure 14 shows the normalized z distributions for K^0, Λ, π^+, and π^-, where the fragmentation variable z is the fraction of the corrected hadronic energy carried by the particle. An interesting difference between the strange particles and the pions is that for the former the z distributions turn over at very low z, while for the latter they continue rising all the way to $z=0$. Such a turnover was also seen by Grassler *et al.*[10] and Allasia *et al.*,[13] but not by Bosetti *et al.*[12] In part the turnover may be due to rest mass effects, especially for the Λ. It should be noted also that vees at very low z would generally have very low energies and poorer detection efficiencies than vees at higher z.

Figure 15 shows the normalized P_T^2 distributions for K^0 and Λ. We confirm the observation of other experiments[10,12] that in the region $0<P_T^2<0.5$ $(\mathrm{GeV}/c)^2$ the data can be described by a simple exponential of the form $A\exp(-BP_T^2)$. Fits to this form are shown in the figure, and yield slope parameters of $B=4.68\pm0.18$ $(\mathrm{GeV}/c)^{-2}$ for the K^0 and $B=4.53\pm0.21$ $(\mathrm{GeV}/c)^{-2}$ for the Λ. These values are in excellent agreement with Bosetti *et al.*[12] and consistent with Grassler *et al.*[10] Above 0.5 $(\mathrm{GeV}/c)^2$ there is a possible change of slope or deviation from simple exponential.

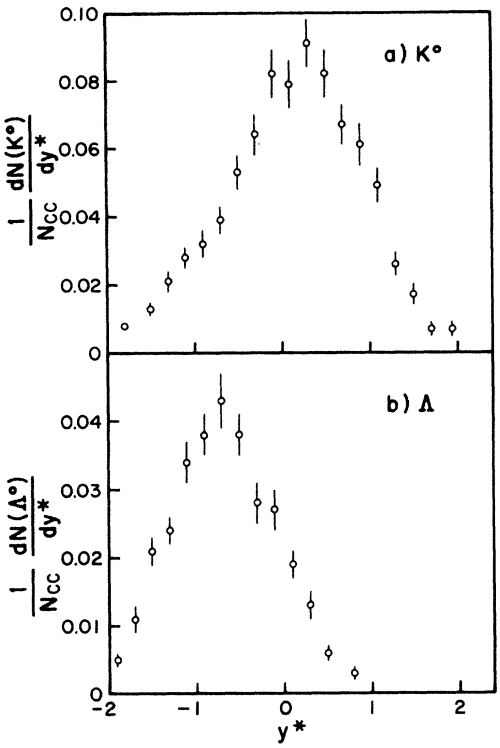

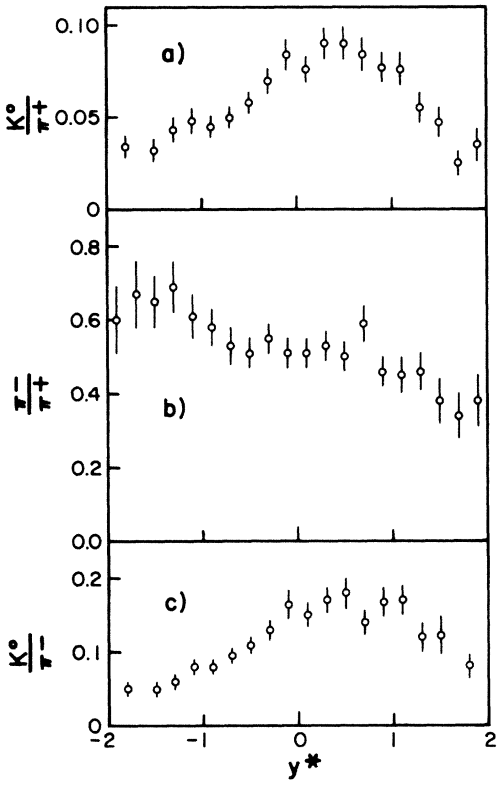

FIG. 13. Ratios of normalized rapidity distributions for (a) K^0/π^+, (b) π^-/π^+, and (c) K^0/π^-.

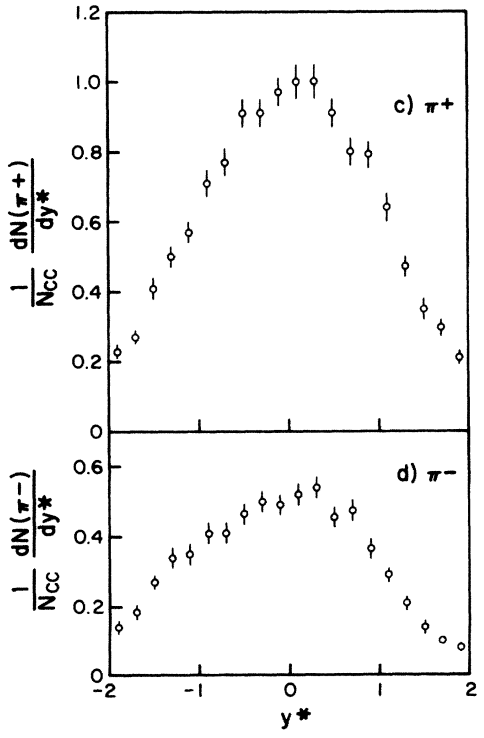

FIG. 12. Normalized center-of-mass rapidity distributions for (a) K^0, (b) Λ, (c) π^+, and (d) π^-. The pions are from the random charged-current sample.

Quantum chromodynamics (QCD) predicts that $\langle P_T^2 \rangle$ should increase with Q^2 and decrease with x_B. It has been pointed out[17] that there is an experimental problem in measuring $\langle P_T^2 \rangle$. Because of undetected neutrals the hadronic system's direction can only be estimated and is sensitive to the energy correction. However, the neutrino-muon plane, sometimes called the lepton plane, is very well determined, and therefore we can accurately measure $\langle P_T^2 \rangle_{\text{out}}$, the square of the momentum component transverse to the lepton plane. We have calculated both variables for K^0 and Λ, and we show their dependence on Q^2, x_B, and W^2 in Figs. 16, 17, and 18, respectively. Neither $\langle P_T^2 \rangle$ nor $\langle P_T^2 \rangle_{\text{out}}$ shows any significant evidence for a variation with Q^2 or x_B. However, there is a clear increase with W^2, at least for the K^0. Ammosov *et al.*[17] have noted that W^2 may be the most sensitive, because $W^2 \sim Q^2(1/x_B - 1)$ so that the QCD prediction is magnified.

VI. Ξ^- PRODUCTION

The production of Ξ^- in neutrino interactions has never been reported. Because the Ξ contains two s quarks, it is not surprising that its cross section is small. Two possible production mechanisms are (a) double associated production (two $s\bar{s}$ quark pairs) and (b) associated production and charm production both occurring. This latter possibility could include the formation of the strange charm baryon Ξ_c, followed by its decay into Ξ^-.

TABLE V. Production properties of K^0, Λ, π^+, and π^-.

	K^0	Λ	π^+	π^-
$A=(N_F-N_B)/(N_F+N_B)$	$+0.16\pm0.02$	-0.71 ± 0.02	$+0.004\pm0.012$	-0.082 ± 0.017
$\langle z\rangle$	0.198 ± 0.003	0.183 ± 0.003	0.132 ± 0.002	0.104 ± 0.002
$\langle P_T\rangle$ (GeV/c)	0.460 ± 0.006	0.463 ± 0.006	0.398 ± 0.004	0.372 ± 0.007
$\langle P_T^2\rangle$ [(GeV/c)^2]	0.269 ± 0.007	0.268 ± 0.007	0.201 ± 0.003	0.166 ± 0.004
$\langle P_T^2\rangle_{\text{out}}$ [(GeV/c)^2]	0.124 ± 0.004	0.129 ± 0.004	0.097 ± 0.002	0.087 ± 0.003
P_T^2 slope [(GeV/c)$^{-2}$]	4.68 ± 0.18	4.53 ± 0.21		

Approximately one-third of the film was scanned for events where a V^0 pointed to a kink on a negative track. Each such event was measured, and in the kinematic analysis the V^0 was fitted as a Λ from the kink vertex. For the events with a successful Λ fit, the kinematic hypothesis $\Xi^-\to\Lambda\pi^-$ was tried with three or four constraints. The events were subjected to the same selection criteria as for the entire SCC sample. However, two additional requirements were imposed: (a) the Ξ was required to have a minimum track length of 1 cm to improve its detection efficiency and to reduce its angle errors for the fit and (b) the muon candidate was required to be not only the fastest negative leaving track, but also the one with the largest transverse momentum with respect to the vector sum of the other track momenta. The purpose of this cut was to reduce the background from K_L interactions in which a π^- might mimic a μ^- by leaving the chamber without interacting. The K_L can be produced by neutrino interactions in the upstream wall of the chamber.

After all these cuts, five events were obtained with a Ξ^- and a muon. Four of these were ν induced, while the fifth was $\bar{\nu}$ induced. To calculate a rate for the four ν events, we used the same procedure as described in Sec. III. The Λ weight was assumed to be the same as for the SCC sample. The weight due to the 1-cm-length cut on the Ξ was calculated for each event by using the fitted Ξ momentum and known decay lifetime. The loss due to the transverse-momentum requirement on the muon was calculated by examining the RCC sample, in which it was found that the muon had the largest transverse momentum 95% of the time. The scan efficiency for finding kinking tracks on events where a V^0 was already found was $(75\pm10)\%$.

The only significant background was due to K_L interactions. Since this is a punch-through background, we followed the same procedure as described in Sec. II to calculate it. In the SCC sample we found that among the had-

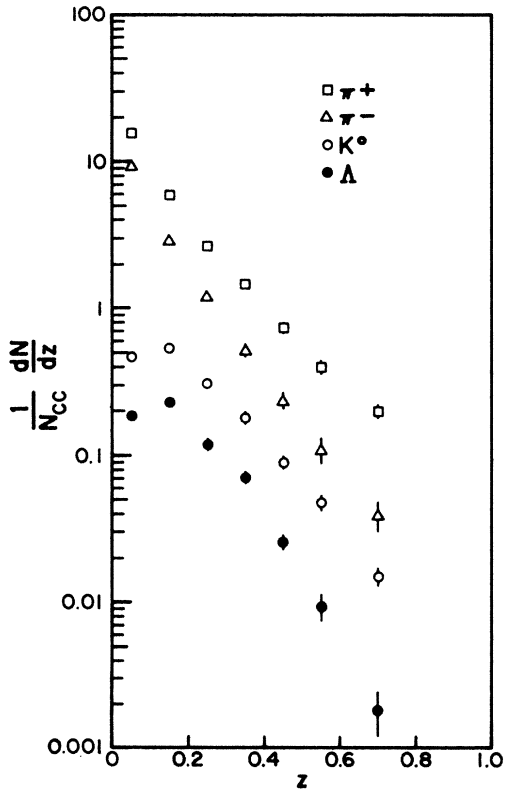

FIG. 14. Normalized distributions in the fragmentation variable z for K^0, Λ, π^+, and π^-. z is the fraction of the corrected hadronic energy carried by the particle. The pions are from the random charged-current sample.

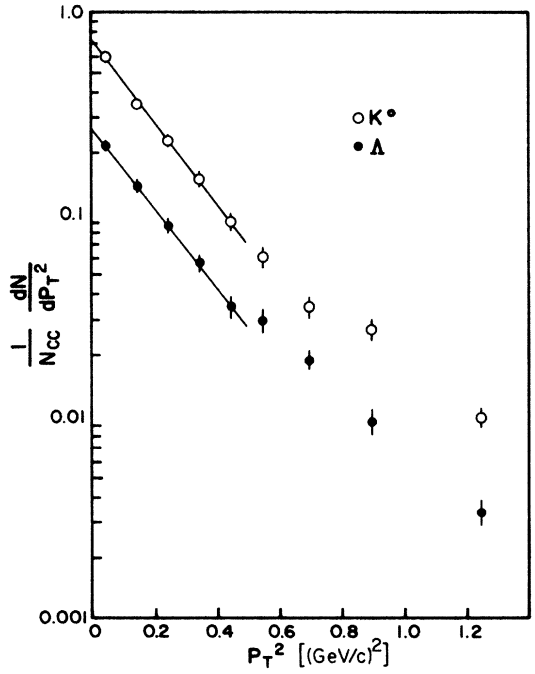

FIG. 15. Normalized distributions in transverse momentum squared for K^0 and Λ. The solid lines are simple exponential fits to the data.

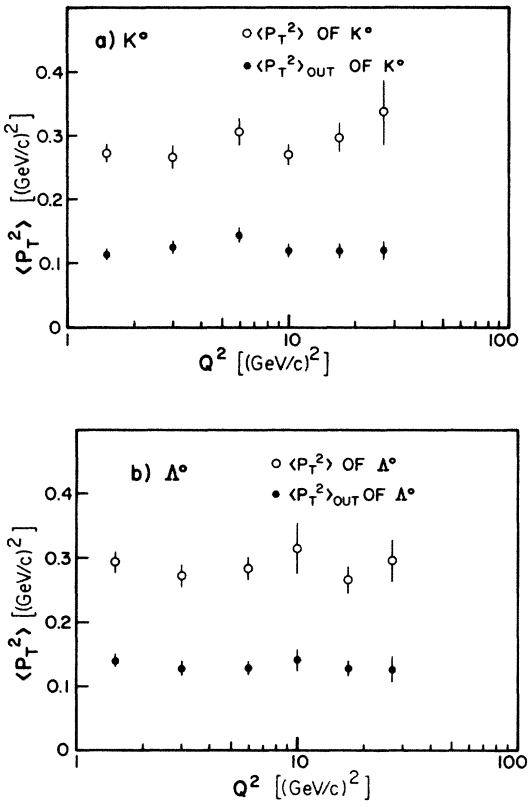

FIG. 16. Average transverse momentum squared as a function of Q^2, the square of the four-momentum transfer from neutrino to muon, for (a) K^0 and (b) Λ. The open circles are for momentum component transverse to the direction of the hadronic system, while the solid circles are for momentum component perpendicular to the neutrino-muon plane.

ron tracks over 2 GeV/c, the number that were leaving were 0.55 times the number interacting. In our Ξ sample there was only a single negative interacting track over 2 GeV/c, so we calculate 0.55 ± 0.55 negative leaving punch-through tracks. The sample contained four negative leaving tracks over 2 GeV/c, one in each ν event, which were the four muon candidates; therefore, the background is 0.55 ± 0.55.

Applying all of these corrections, the rate for charged-current ν production of Ξ^- is

$$\frac{R(\nu_\mu+\mathrm{Ne}\rightarrow\mu^-+\Xi^-+\cdots)}{R(\nu_\mu+\mathrm{Ne}\rightarrow\mu^-+\cdots)}=(6\pm4)\times10^{-4}.$$

It is noteworthy that this rate is comparable within errors to the rate for $\Lambda\Lambda$ production (see Table III). The possible production mechanisms for the $\Lambda\Lambda$ channel, mentioned at the end of Sec. IV, are the same as for the Ξ, namely double associated production of two $s\bar{s}$ pairs, or single associated production plus charm.

Table VI summarizes the important features of the Ξ^- events. Three of the four ν-induced events are rather similar to each other, and the Ξ properties are very much like those of the Λ in the SCC sample. Feynman x and rapidity for the Ξ both suggest the target-fragmentation

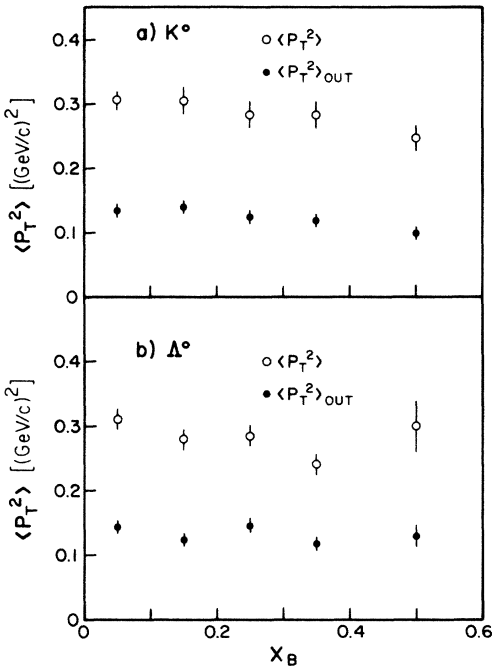

FIG. 17. Average transverse momentum squared as a function of x_B, the fraction of the nucleon momentum carried by the struck quark, for (a) K^0 and (b) Λ. The open circles are for momentum component transverse to the direction of the hadronic system, while the solid circles are for momentum component perpendicular to the neutrino-muon plane.

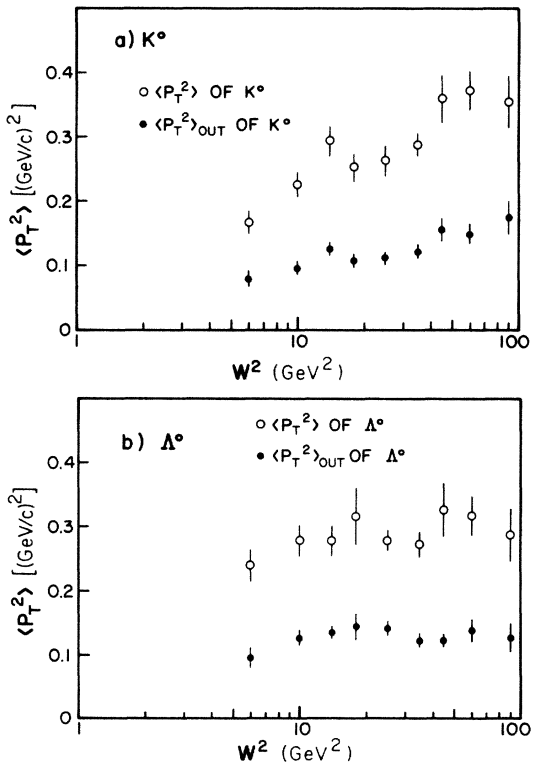

FIG. 18. Average transverse momentum squared as a function of W^2, the corrected hadronic effective mass squared. The open circles are for momentum component transverse to the direction of the hadronic system, while the solid circles are for momentum component perpendicular to the neutrino-muon plane.

TABLE VI. Properties of Ξ^- events.

	Event 1	2	3	4	5
Incident beam	ν	ν	ν	ν	$\bar{\nu}$
E_ν (GeV)	100.5	15.7	21.1	23.8	37.5
Q^2 [(GeV/c)^2]	4.1	2.5	1.2	4.6	2.3
W^2 [(GeV)^2]	50.3	22.8	33.5	17.1	11.3
x_B	0.08	0.10	0.04	0.22	0.18
y_B	0.28	0.83	0.85	0.47	0.18
$P(\Xi)$ (GeV/c)	11.4	2.0	1.4	1.9	3.5
$x_F(\Xi)$	0.29	−0.57	−0.75	−0.59	0.14
$y^*(\Xi)$	0.68	−0.78	−1.15	−0.74	0.17
$P_T{}^2(\Xi)$ [(GeV/c)^2]	0.25	0.76	0.57	0.51	0.19
$z(\Xi)$	0.39	0.17	0.10	0.19	0.48

process that characterizes the Λ, while transverse momentum is higher for the Ξ than the Λ. However, event No. 1 in the table is strikingly different. It is an event of very high ν energy, in which the Ξ is clearly going forward in the hadronic center of mass, not in the target region. Furthermore, the Ξ carries 39% of the hadronic energy, although it is one of six charged hadrons in the event.

The Ξ events were examined to see if mass combinations of the particles in the hadronic final states were consistent with the strange charm baryons Ξ_c^0 or Ξ_c^+ using the observed[18] mass 2.46 GeV/c^2. None of the events could be interpreted this way. The 90%-confidence-level upper limit on the cross section for producing the Ξ_c, times the branching ratio for the decay of Ξ_c to Ξ^- plus charged pions, is 4×10^{-4}, expressed as a fraction of the cross section for all charged-current events.

VII. CONCLUSIONS

We have studied strange-particle production in ν_μNe charged-current interactions, using a sample of 4215 fitting vees, corresponding to 61 800 charged-current events. This is a significantly larger vee sample than has previously been reported. Inclusive V^0 production rates as a fraction of all charged-current events are measured to be 0.168 ± 0.012 for the K^0, 0.065 ± 0.005 for the Λ, $(4.6\pm0.8)\times10^{-3}$ for the $\bar{\Lambda}$, 0.011 ± 0.003 for the Σ^0, and $(5.8\pm3.6)\times10^{-4}$ for the Ξ^-. The ratio of the Λ to K^0 rate is 0.39 ± 0.04. The fraction of Λ coming from Σ^0 decay is $(16\pm5)\%$.

Rates were also measured for single-, double-, and triple-V^0 production. From these we determined that associated production of an $s\bar{s}$ quark pair occurs at a $(19.5\pm1.4)\%$ rate in ν charged-current interactions, while single-s-quark production (via charm) occurs at a $(5.0\pm1.5)\%$ rate.

The production of K^0 increases sharply with E_ν, Q^2, W^2, and y_B, but is independent of x_B. Production of Λ is essentially independent of all these variables. These results suggest that the K^0 is produced in the current jet, while the Λ comes from target fragmentation. This conclusion is corroborated by the Feynman-x and rapidity distributions. The forward-backward asymmetry parameter is $+0.16\pm0.02$ for the K^0 and -0.71 ± 0.02 for the Λ. The K^0/π^+ ratios as a function of x_F and y^* provide striking evidence for enhanced production of K^0 in the forward region relative to π^+. z distributions for K^0 and Λ both show a turnover at small z.

The $P_T{}^2$ distributions for K^0 and Λ can be described by simple exponentials below 0.5 (GeV/c)^2, with slopes of -4.68 ± 0.18 (GeV/c)$^{-2}$ for the K^0 and -4.53 ± 0.21 (GeV/c)$^{-2}$ for the Λ. Neither $\langle P_T{}^2\rangle$ nor $\langle P_T{}^2\rangle_{\text{out}}$ shows significant variation with Q^2 or x_B, as predicted by QCD. However, an increase with W^2 is clearly observed.

ACKNOWLEDGMENTS

We thank the scanning and measuring staffs at our institutions, and the operating crews of the 15-ft chamber and the neutrino beam at Fermilab. This research was supported by the Department of Energy (Contract No. DE-AC02-76CH00016) and by the National Science Foundation.

*Present address: Bear, Stearns, and Co., New York, NY.
†Deceased.
‡Present address: IBM Research Center, Yorktown Heights, NY 10598.
§Present address: AT&T Bell Laboratories, Allentown, PA 18103.
**Present address: Princeton University, Princeton, NJ 08544.
††Present address: CERN, Geneva, Switzerland.

[1]N. J. Baker *et al.*, Phys. Rev. D **32**, 531 (1985).
[2]C. Baltay *et al.*, Phys. Rev. Lett. **41**, 73 (1978).
[3]C. Baltay *et al.*, Phys. Rev. Lett. **42**, 1721 (1979).
[4]A. Grant, Nucl. Instrum. Methods **127**, 355 (1975).
[5]Particle Data Group, Rev. Mod. Phys. **56**, S1 (1984).
[6]H. Deden *et al.*, Phys. Lett. **58B**, 361 (1975).
[7]J. P. Berge *et al.*, Phys. Rev. Lett. **36**, 127 (1976).
[8]J. P. Berge *et al.*, Phys. Rev. D **18**, 1359 (1978).
[9]N. J. Baker *et al.*, Phys. Rev. D **24**, 2779 (1981).
[10]H. Grassler *et al.*, Nucl. Phys. **B194**, 1 (1982).

[11]R. Brock *et al.*, Phys. Rev. D **25**, 1753 (1982).
[12]P. Bosetti *et al.*, Nucl. Phys. **B209**, 29 (1982).
[13]D. Allasia *et al.*, Nucl. Phys. **B224**, 1 (1983).
[14]O. Erriquez *et al.*, Nucl. Phys. **B140**, 123 (1978).
[15]V. V. Ammosov *et al.*, Nucl. Phys. **B177**, 365 (1981).
[16]For further details, see L. Chen, Ph.D. thesis, Columbia University, Nevis Report No. 246, 1984.
[17]V. V. Ammosov *et al.*, Nucl. Phys. **B162**, 205 (1980).
[18]S. F. Biagi *et al.*, Phys. Lett. **122B**, 455 (1983).